ACS OMEGA

http://pubs.acs.org/journal/acsodf

Article

Hydrothermal Aging Mechanism and Modeling for SCR Catalysts

Dongwei Yao,* Xiaohan Hu, Feng Wu, Xingwen Li, and Yuxi Li

Cite This: *ACS Omega* 2023, 8, 2421−2434

Read Online

ACCESS | Metrics & More | Article Recommendations

ABSTRACT: Based on the activity evaluation and characterization test, we explored the hydrothermal aging mechanism of a vanadium-based SCR catalyst and constructed a dual-site hydrothermal aging kinetic model in this study. The vanadium-based catalyst contains Brønsted acidic sites and Lewis acidic sites, which show different sensitivities to hydrothermal aging, and the reduction of active sites is the main reason for the NO*x* conversion efficiency reduction after hydrothermal aging. The ammonia storage capacities of both sites have a high correlation coefficient with the NO*x* conversion efficiency. Based on the method of NH_3-TPD curve peak resolution, we quantified the transformations of the two active sites and established the relationship between the site density, the aging temperature, and the duration to determine the aging factor. Then, a hydrothermal aging kinetic model was constructed, and the parameter identification and verification of the model were carried out through flow reactor experiments. The results show that the model constructed in this study can accurately reflect the catalyst activity after hydrothermal aging.

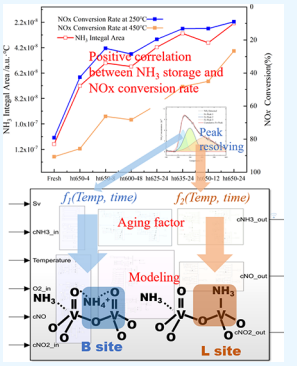

1. INTRODUCTION

Diesel engines are still irreplaceable due to their advantages such as excellent power, high reliability, and excellent fuel economy,[1] but the regulations on the NO*x* emitted by diesel are becoming stricter. The diesel engine after-treatment system widely uses ammonia-selective catalytic reduction (NH_3-SCR) technology to reduce NO*x* emissions.[2,3] At present, there are many types of catalysts used in SCR. The vanadium-based catalyst that has been widely used for decades possesses high activity, excellent sulfur resistance, low fuel quality requirement, good product maturity, and low cost.[4,5] Therefore, even under strict emission regulations, there are still great application prospects in power plants, ships, agricultural machinery, and heavy vehicles.[6,7]

As a result of the relatively poor hydrothermal stability of the vanadium-based SCR catalyst used in conjunction with DPF, high-temperature thermal shock caused by the active regeneration of DPF will increase the risk of hydrothermal aging of the vanadium-based SCR catalyst.[8] Although the state-of-the-art vanadium-based SCR catalyst has high temperature tolerance, which has been successfully used in systems with exhaust temperatures up to 650 °C and certain European OEM applications,[9] the irreversible negative effects of high-temperature hydrothermal aging on the SCR reactivity of the vanadium-based SCR catalyst will gradually accumulate over time. Therefore, it is essential to study the hydrothermal aging mechanism and establish a hydrothermal aging model to improve the hydrothermal stability and predict the service life of the vanadium-based SCR catalyst.

There have been extensive studies on the hydrothermal aging mechanism of vanadium-based SCR catalysts. Xi et al.[10] found that an increase in the hydrothermal aging temperature not only led to the reduction of the BET specific surface area and BJH pore volume of the catalyst but also caused the formation of cracks in the base coating. Madia et al.[11] also proposed that the degradation of catalyst performance was due to the reduction of the specific surface area and the generation of multilayer crystalline vanadium after hydrothermal aging. Beale et al.[12] believed that the hydrothermal aging mechanisms of vanadium-based catalysts included the sintering and phase change of anatase, the conversion of highly dispersed WO_3 to monoclinic WO_3, and the conversion of polymerized V_2O_5 to V_2O_5 crystals. Went et al.[13] found that oligomeric vanadium has great SCR activity and N_2 selectivity. The decrease in SCR activity was mainly due to the lower activity of highly polymerized vanadium and vanadium crystals. The conclusion that vanadium was converted into V_2O_5 crystals is currently supported by many scholars.[11,12,14−19] Other scholars have found that in the process of hydrothermal aging, the inevitable phase transition from anatase to rutile is included as a deactivation factor.[9,12,15,20] Choung et al.[15] believed that the reduction of the BET specific surface area was caused by the sintering and phase transition of anatase, and Nova et al.[21] believed that the sintering of anatase can lead to the agglomeration of vanadium. Madia et al.[11] also mentioned that sintering can cause an increase in the types of polyvanadium. In general, current researchers believe that the

Received: October 26, 2022
Accepted: December 16, 2022
Published: January 2, 2023

https://doi.org/10.1021/acsomega.2c06902
ACS Omega 2023, 8, 2421−2434

reduction of specific surface area, the agglomeration of vanadium, and the sintering and phase change of the TiO_2 support during hydrothermal aging are the main reasons for the deactivation of vanadium-based catalysts during hydrothermal aging.

The widely accepted and applied SCR reaction mechanism of vanadium-based catalysts is proposed by Ramis and Topsøe. Ramis et al.[22] proposed that NH_3 was adsorbed on the Lewis acidic position to form an amino compound and then decomposed to form an intermediate with gaseous NO. Finally, N_2 and H_2O were produced in the presence of the catalyst, and vanadium oxide underwent redox reactions during the entire process. Topsøe et al.[23,24] believed that NH_3 was adsorbed on V_5^+-OH to form an ammonium ion with a Brønsted acidic site and then reacted with gaseous NO to form an intermediate, and the intermediate was finally decomposed into N_2 and H_2O. During the entire reaction, the ortho $V_5^+ = O$ was first reduced to V_4^+-OH and then oxidized into $V_5^+ = O$ by the gaseous O_2. In addition, Minghui et al.[25] studied the ammonia distribution and reaction mechanisms of the Lewis and Brønsted acidic sites on the surface and found that both of the sites were involved in the SCR reaction. Hanzi et al.[26] further proposed that the Lewis acidic position was critical at high reaction temperatures, while the Brønsted acid dominated the entire reaction at lower temperatures, and the surface Lewis acid sites were converted to Brønsted acid sites at high temperature and in the presence of water vapor. Song et al.[27] found that the Brønsted and Lewis acidic sites could transform into each other. In general, with the deepening of research, our understanding of the reaction mechanism of vanadium-based SCR is constantly improving, and the points of controversy are gradually becoming clear. However, in the process of hydrothermal aging, the changes in the two active sites still need to be further studied.

Although the reaction mechanism based on the dual active sites and different sensitivities of different active sites to temperature has gradually become a fact, the current kinetic models for vanadium-based catalysts are dominated by single-active-site models. Nova et al.[28−30] and Tronconi et al.[31,32] established single-site SCR reaction models and gave a complete and detailed description of the NH_3-SCR reaction. In recent years, the models of V_2O_5/TiO_2 catalysts established by Yun et al.,[33] Lothongkum et al.,[34] Yu et al.,[35] Usberti et al.,[36] Beretta et al.,[37] Shin et al.,[38] Xiong et al.,[39] and Soleimanzadeh et al.[40] according to different research purposes and application scenarios are all single-active-site models. In our previous study, a hydrothermal aging mechanism based on dual active sites was proposed,[41] so it is reasonable and necessary to establish a dual-active-site model. In addition, there are not many studies on the hydrothermal aging model of SCR catalysts. Bartley et al.[42] studied the thermal aging of V_2O_5-WO_3/TiO_2 and copper- and iron-based SCR catalysts and used the NH_3 storage capacity to characterize the degree of catalyst deactivation. Kim et al.[43] obtained the axial deactivation coefficient reflecting the aging of the catalyst for a metal−zeolite SCR catalyst. Kim et al.[44] established an axial hydrothermal aging model of vanadium-based catalysts to simulate road aging of 120,000 miles. Supriyanto et al.[45] established a hydrothermal aging model on Cu-zeolites using two aging factors to represent the degrees of hydrothermal aging of the two active sites at different temperatures.

In summary, there are still considerable shortcomings in the reaction kinetic models of vanadium-based catalysts, especially the models with the hydrothermal aging mechanism. Attention should be paid to the changes in active sites during hydrothermal aging. Different active sites have different temperature ranges of activity, which is still not reflected in the models, so it is significant to establish a reasonable reaction kinetic model with the hydrothermal aging mechanism. In this study, a commercial vanadium-based catalyst was used as the object, and activity evaluation and characterization tests such as XRD, BET, and NH_3-TPD were carried out. The hydrothermal aging characteristics and microscopic mechanism of hydrothermal aging of the vanadium-based catalyst were analyzed, especially the hydrothermal aging mechanism of different active sites and their effects on the ammonia storage capacity. On this basis, a hydrothermal aging model of dual active sites was modeled, and the parameters were identified and verified. This model provides a theoretical basis for the prediction and evaluation of the activity and durability of vanadium-based catalysts.

2. EXPERIMENTAL SECTION

2.1. Catalyst Preparation. The catalyst used in the experiment was a commercial V_2O_5-WO_3/TiO_2 catalyst containing 2.45% V_2O_5, 9.6% WO_3, and 86.6% TiO_2. The catalyst was prepared by the incipient wetness impregnation method. First, oxalic acid and NH_4VO_3 were dissolved in pure water, and the mixture was stirred for 30 min. Thereafter, anatase TiO_2 and WO_3 powder were added, and then the mixture was stirred for 1.5 h. Thereafter, the mixture was dried and ground carefully. Finally, the obtained powder was calcined for 3 h at 550 °C. The powder was tableted and sieved through 40−60 meshes before the test.

2.2. Flow Reactor Experiments. A flow reactor system was used for catalyst deactivation, activity evaluation, and NH_3-TPD in this study. The catalyst was placed in a quartz tube of a tube furnace, the inlet gas composition was controlled by mass flow controllers, and the outlet gas composition was analyzed by an MKS Multi-gas 6030 FTIR spectrometer. For the uniformity of flow and the consistency of results, each test sample is composed of 100 mg of catalyst (40−60 mesh) mixed with 50 mg of quartz san.

2.2.1. Hydrothermal Aging. To acquire hydrothermally aged vanadium-based catalysts, fresh catalysts were initially activated in a standard SCR atmosphere at 550 °C for 1 h to improve the adaptability and tolerance of the catalyst. The gas hourly space velocity (GHSV) was 120,000 h^{-1}, and the gas composition was 300 ppm NO, 300 ppm NH_3, 10% O_2, 7% H_2O, and balanced with N_2. Then, the catalyst was purged with 10% O_2, 7% H_2O, and balanced with N_2 at 550 °C for 30 min to remove impurities. Thereafter, the catalysts underwent a hydrothermal aging treatment with a gas consisting of 300 ppm NO, 300 ppm NH_3, 10% O_2, 7% H_2O, and balanced with N_2. The aging temperature and aging time are shown in Table 1. Fresh samples are marked as "fresh", and aging samples are marked as "ht+Temperature-time". For example, "ht600-15" means a sample that has been hydrothermally aged at 600 °C for 15 h.

2.2.2. XRD Studies. Phase transformation and sintering of vanadium-based catalysts during hydrothermal aging were characterized by XRD, which was performed on a PANalytical X'Pert^3 diffractometer. Samples were scanned from 10 to 80° (2θ) in steps of 0.02° s^{-1} with a Cu Ka anode (λ = 0.015405 nm) at 40 kV and 40 mA. The calculation of the crystallite dimension D was based on the Scherrer equation

https://doi.org/10.1021/acsomega.2c06902
ACS Omega 2023, 8, 2421−2434

Table 1. Hydrothermal Aging Treatment Conditions

sample	aging temperature/°C	aging time/h
fresh		
ht580-15	580	15
ht600-15	600	15
ht615-15	615	15
ht625-15	625	15
ht630-15	630	15
ht635-3	635	3
ht635-6	635	6
ht635-9	635	9
ht635-11	635	11
ht635-12	635	12
ht635-15	635	15
ht650-4	650	4
ht650-8	650	8
ht650-12	650	12
ht650-24	650	24
ht600-48	600	48
ht625-24	625	24
ht635-24	635	24
ht-diff-tT	600 °C 6 h + 625 °C5 h + 650 °C 4 h	

$$D = \frac{k_d \lambda}{\beta \cos \vartheta} \quad (1)$$

where k_d is a constant depending on the particle shape, λ is the wavelength of the X-ray radiation, β is the full width at half-maximum (FWHM) of the diffraction peak, and ϑ is the diffraction angle.

After the phase transition, the content X_R (%) of the rutile-phase TiO_2 in the aged sample was calculated as follows

$$X_R = (1 + 0.794 I_a/I_r)^{-1} \quad (2)$$

where I_a and I_r are the measured intensities of the (101) and (110) plane reflections for anatase and rutile, respectively.

2.2.3. BET Studies. The specific surface area of the catalyst samples was determined by liquid nitrogen adsorption. The samples were vacuum pretreated at 150 °C for 12 h, and then, the N_2 adsorption isotherms of the BET surface area at 77 K were recorded by a Micromeritics Trista II instrument.

2.2.4. NH_3-TPD Studies. NH_3-TPD was used to characterize the ammonia storage of fresh catalysts and hydrothermally aged catalysts. For each sample, the adsorption was performed by exposing it to a feed of 300 ppm NH_3, 7% H_2O, and balanced with N_2 at 100 °C for 1.5 h. Then, the NH_3 was shut off and the sample was purged at the adsorption temperature for 1.5 h to remove the physically adsorbed NH_3. During the desorption process, the temperature of the sample was increased at a constant heating rate of 10 °C/min to 600 °C. All samples were tested several times, and the results were completely consistent. The NH_3 desorption curve of the TPD process was integrated, and the integrated area can be considered as the ammonia storage of the sample.

2.2.5. Performance Evaluation. After each aging, a performance evaluation test was conducted, and its steps were as follows: NO oxidation, NH_3 adsorption, NH_3 oxidation, NH_3 desorption, and standard SCR reaction. The steps were conducted using 300 ppm NO (if needed), 300 ppm NH_3 (if needed), 10% O_2, 7% H_2O, and balanced with N_2, and the space velocity was 300,000 h^{-1}. The detailed gas concentrations and steps of the reaction kinetics test are shown in Table 2. The steps above were performed repeatedly at every 50 °C from 200 to 450 °C.

The NO*x* conversion rate and NH_3 oxidation rate in the standard SCR reaction were calculated as follows

$$\text{NO}x \text{ conversion rate} = \frac{C_{NO_{in}} - C_{NO_{out}} - C_{NO_{2out}}}{C_{NO_{in}}} \quad (3)$$

$$NH_3 \text{ conversion rate} = \frac{C_{NH_{3in}} - C_{NH_{3out}}}{C_{NH_{3in}}} - \text{NO}x \text{ conversion rate} \quad (4)$$

where $C_{NO_{in}}$ and $C_{NH_{3in}}$ are the concentrations of NO and NH_3 at the inlet of the catalyst sample, respectively; $C_{NO_{out}}$, $C_{NO_{2out}}$, and $C_{NH_{3out}}$ are the concentrations of NO, NO_2, and NH_3 at the outlet of the catalyst sample, respectively.

3. RESULTS AND DISCUSSION

3.1. Hydrothermal Aging Mechanism. *3.1.1. NOx Conversion Efficiency Analysis.* As shown in Figure 1, the fresh catalysts exhibit good activity and a wide temperature window. The NO*x* conversion rate can reach 79.06% at 250 °C and 90.4% at 450 °C. However, for the aged catalyst samples, the NO*x* conversion rate decreased sharply, and the temperature window was greatly reduced during the hydrothermal aging process. In vanadium-based catalysts, there are Brønsted acid sites and Lewis acid sites with different characterizing positions, and both of them are involved in the SCR reaction. The active sites at different positions have different stabilities during the hydrothermal aging process, and with the deepening of the aging degree, catalyst surface remodeling will occur. The different sensitivities of the two active sites to hydrothermal aging result in different relative deactivation degrees of active sites at low temperatures and high temperatures after hydrothermal aging. The relative deactivation of the sample is defined by dividing the difference between the conversion efficiencies of the fresh and aged samples by the conversion efficiency of the fresh sample. As shown in Figure 2, the relative deactivation degrees of the NO*x* conversion efficiency in the low-temperature (around 250 °C) and high-temperature (around 450 °C) segments are obviously stratified, which may

Table 2. Performance Evaluation Test Procedure

sample	NO oxidation	NH_3 adsorption	NH_3 oxidation	NH_3 desorption	standard SCR
time/min	25	30	20	30	35
NO/ppm	300	0	0	0	300
NH_3/ppm	0	300	300	0	300
O_2/%	10	0	10	10	10
H_2O/%	7	7	7	7	7

https://doi.org/10.1021/acsomega.2c06902
ACS Omega 2023, 8, 2421−2434

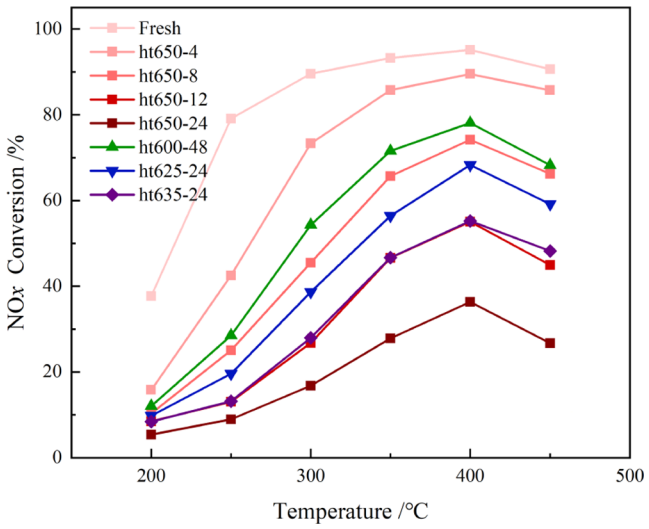

Figure 1. NOx conversion rates of all of the hydrothermally aged samples; 300 ppm NO, 300 ppm NH_3, 10% O_2, 7% H_2O, and balanced with N_2; space velocity = 3×10^5 h^{-1}.

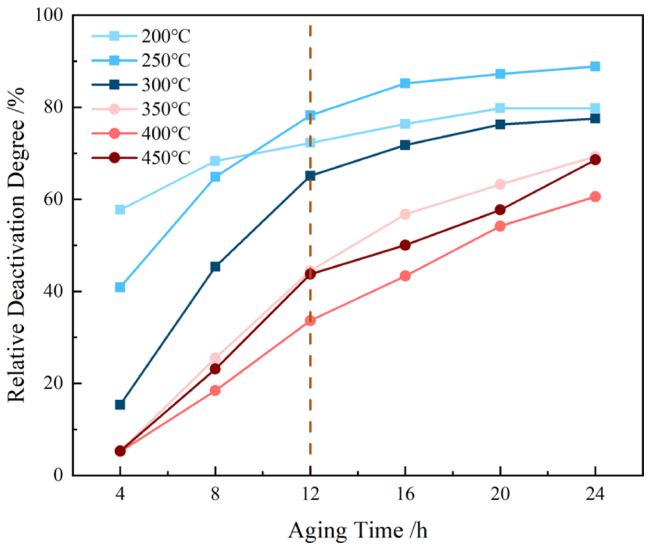

Figure 2. Relative deactivation degrees of all hydrothermally aged samples.

be related to the difference in the active sites that dominate the reaction at low temperatures and high temperatures. The low-temperature reaction is mainly dominated by the Brønsted acid site, and the high-temperature reaction is mainly dominated by the Lewis acid site.[26] Therefore, 250 °C is selected to represent the conversion efficiency at the low-temperature stage and 450 °C to represent the conversion efficiency at the high-temperature stage, and the relationship between the activities of the two active sites and the hydrothermal aging mechanism is determined. The latest research generally suggests that the sintering and phase transformation of the TiO_2 support, the reduction of the specific surface area, and the agglomeration of vanadium during the hydrothermal aging process of vanadium-based catalysts are the main reasons for the loss of activity. The relationship between the degree of relative deactivation and the above hydrothermal aging mechanism will be discussed.

3.1.2. Catalytic Characterization Analysis. The phase transition and particle size growth of the catalyst were studied by XRD experiments, and the results are shown in Figure 3. When vanadium-based catalysts undergo carrier sintering and phase transformation during hydrothermal aging, the anatase grain size and phase transformation ratio will gradually increase with the aging degree. Based on eqs 1 and 2, the crystallite size of TiO_2 and the content of rutile TiO_2 in the phase-transformed samples are obtained. As shown in Figure 4, for samples with the same hydrothermal aging time, such as ht625-24, ht635-24, and ht650-24, the crystallite size of TiO_2 increases from 45.73 to 50 and finally to 59 nm. The phase transformation proportion of rutile is significantly affected by the degree of aging, and it increases with the aging temperature and time. The phase transition ratios of ht625-24 and ht635-24 are 1.19 and 4.68%, respectively, while that of ht650-24 suddenly increases to 29.23%. Therefore, the phase transition of TiO_2 is more likely to occur at relatively high temperatures. Besides, the relationship between the particle size of anatase grains and the catalyst conversion efficiency exhibits an obvious negative correlation, as shown in Figure 4.

The reduction of BET surface area is also one of the main reasons for the decrease in the conversion rate after hydrothermal aging. For the samples with the same aging temperature and different aging degrees, the BET specific surface area decreases from 44 m^2/g of ht650-4 to 20 m^2/g of ht650-8 and finally to 5 m^2/g of ht650-24. As shown in Figure 5, there is a significant positive correlation between the BET specific surface area and the NOx conversion rate at 250 and 450 °C, and the correlation coefficient at 450 °C is slightly lower than that at 250 °C.

3.1.3. Ammonia Storage Performance Analysis. The desorption peak area of NH_3-TPD can help characterize the ammonia storage capacity of the active sites over vanadium-based catalysts. As shown in Figure 6, the NH_3 desorption peak of the fresh catalyst is the highest, and the peak value of the sample after hydrothermal aging gradually decreases with aging time and increasing temperature, and the corresponding integral area of the NH_3 desorption peak also decreases continuously after aging, which means that the ammonia storage capacity decreases continuously during aging. In addition, for the hydrothermally aged samples at the same temperature in Figure 6a, as the aging time increases, the NH_3 desorption peak has a tendency to move to high-temperature regions, but it does not have a linear relationship with the aging time. This phenomenon is also found by comparing the samples with the same aging time and different aging temperatures, as shown in Figure 6b. This is because the characterization of different active sites in vanadium-based catalysts is related to the location and morphology of the active sites. Therefore, when there is more than one active site involved in the reaction, the change in the desorption peaks comprehensively presented by multiple active sites can express the change rule of the active sites during the hydrothermal aging process to a certain extent.

The different temperatures corresponding to the desorption peak indicate the strength of active sites. In this study, the number of catalyst active sites was determined by the area of the desorption peak, and the different active sites were distinguished by resolving NH_3 desorption curve, which has been applied in some studies.[46] As shown in Figure 7, the Gaussian peaks of the NH_3-TPD curve were divided into three peaks at around 200 °C, around 300 °C, and around 400 °C. The fit of the peak resolution results for all samples is over 99%. Then, the relationship between the decreasing trend of ammonia storage and the decreasing trend of NOx conversion

https://doi.org/10.1021/acsomega.2c06902
ACS Omega 2023, 8, 2421−2434

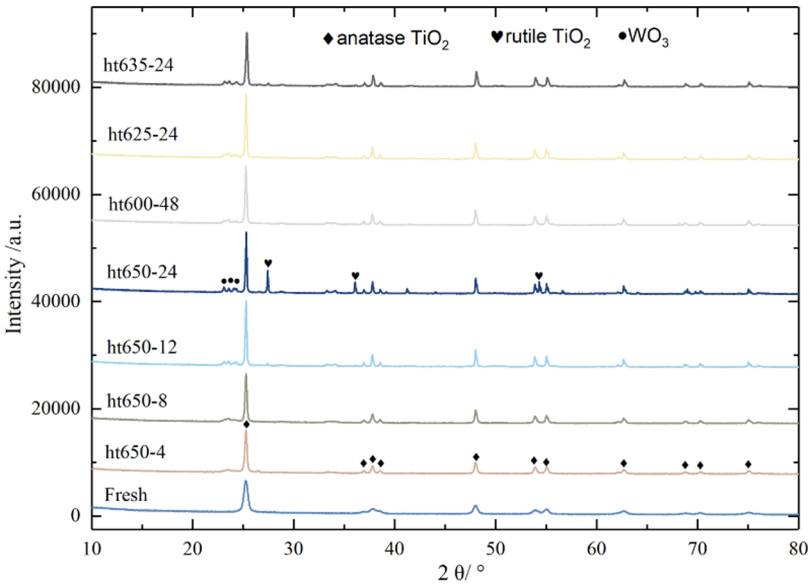

Figure 3. Analysis of the XRD pattern and crystal phase for all hydrothermally aged samples.

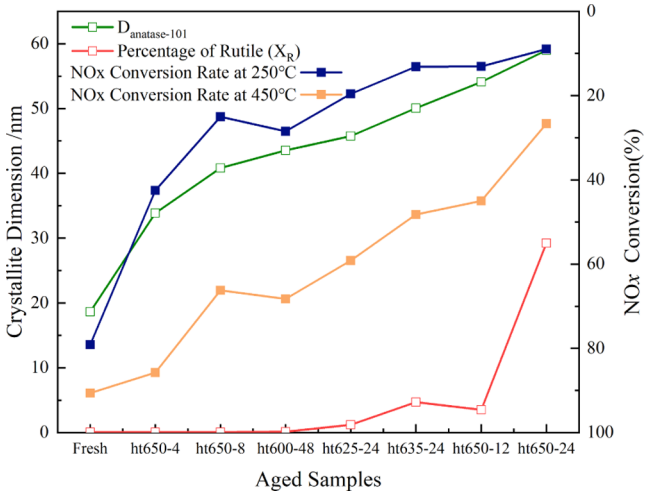

Figure 4. Comparison of the anatase diameter, percentage of phase transformation, and NO*x* conversion rate.

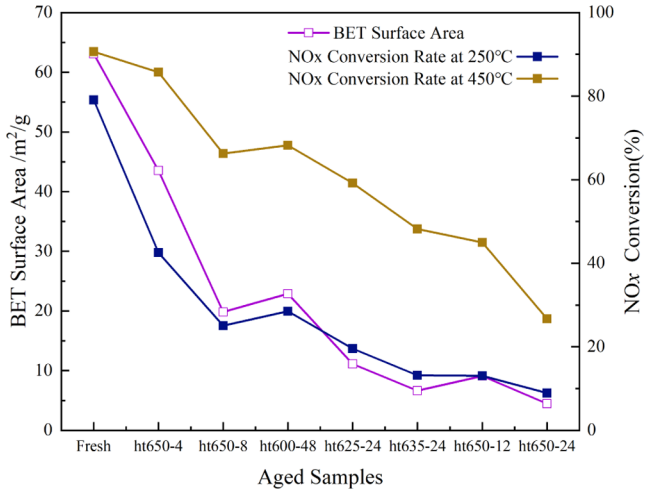

Figure 5. Comparison of the specific surface area and the NO*x* conversion rate.

was compared, as shown in Figure 8. The particle size, specific surface area, and NH_3 storage capacity of the catalyst can reflect the change in the active site of the vanadium-based catalyst after hydrothermal aging to a certain extent. In this study, the cosine similarity was selected to calculate the relationship between these values and the conversion efficiency, and the results are shown in Table 3. The NH_3-TPD integral area, which indicates the ammonia storage volume, shows the highest correlation in both the low-temperature and high-temperature sections. On the one hand, the NH_3 storage characteristics of the catalyst are directly determined by the number of active sites and the strength of activity; on the other hand, according to the E−R mechanism, NH_3 adsorption is also a crucial step in the SCR reaction of the catalyst, so it can be said that the conversion efficiency of the catalyst is directly affected by the number of active sites. When the catalyst is severely deactivated, the number of active sites is seriously insufficient, which will make the conversion efficiency extremely low.

3.2. Kinetic Modeling with Hydrothermal Aging.

3.2.1. Hydrothermal Aging Factor Modeling. As a result of the highest correlation between ammonia storage and the NO*x* conversion efficiency, the change in ammonia storage during aging was used in this study as an aging factor linking the aging mechanism to the global kinetic model. Based on the NH_3-TPD characterization test, the different active sites were identified by the corresponding temperature of the desorption peaks, and the number of active sites was characterized by the area of the desorption peak.[47] Therefore, the different active sites were distinguished by resolving the NH_3 desorption curves, referring to previous studies.[46,48]

Regarding the V_2O_5/TiO_2 catalyst, the Brønsted active site is a weak acidic site, while the Lewis acid site is a strong acidic site.[49] Our previous study reported that in the process of hydrothermal aging, the deactivation rules below 350 °C and above 350 °C are obviously different.[41] Therefore, the peak area below 350 °C is regarded as active site 1 (S1), and S1 is a combination of weak acidic sites and medium-strong acidic sites.[26,50] The peak area above 350 °C is regarded as active site 2 (S2), and S2 is the Lewis acid site.

https://doi.org/10.1021/acsomega.2c06902
ACS Omega 2023, 8, 2421−2434

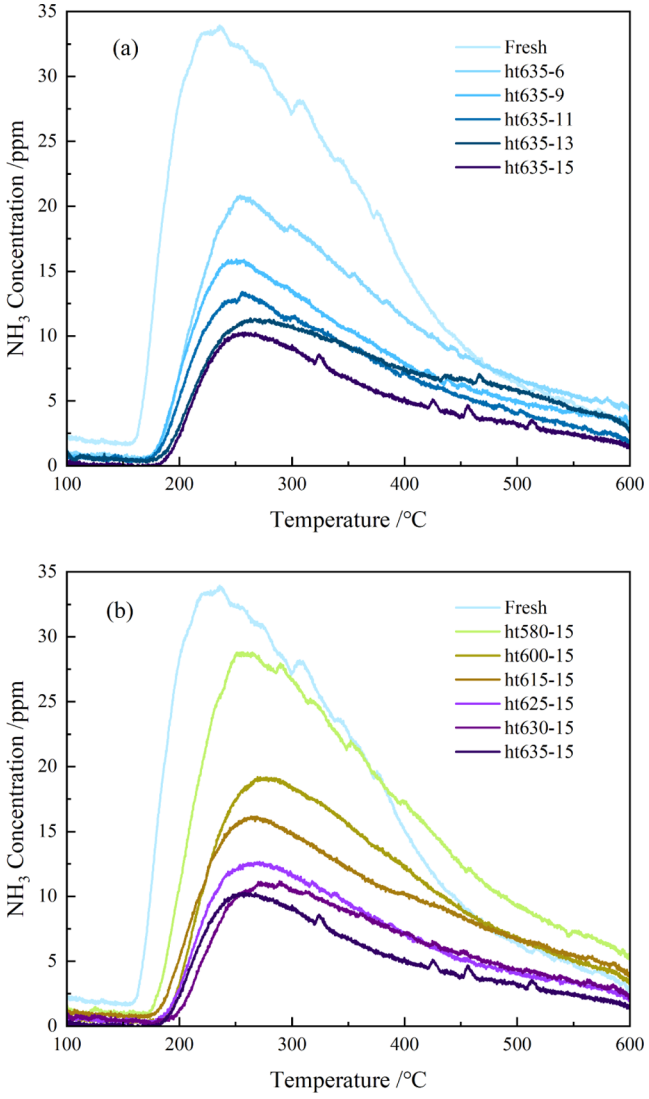

Figure 6. Results of the ammonia storage determination test of all hydrothermally aged samples: (a) samples with different hydrothermal aging times; (b) samples with different hydrothermal aging temperatures.

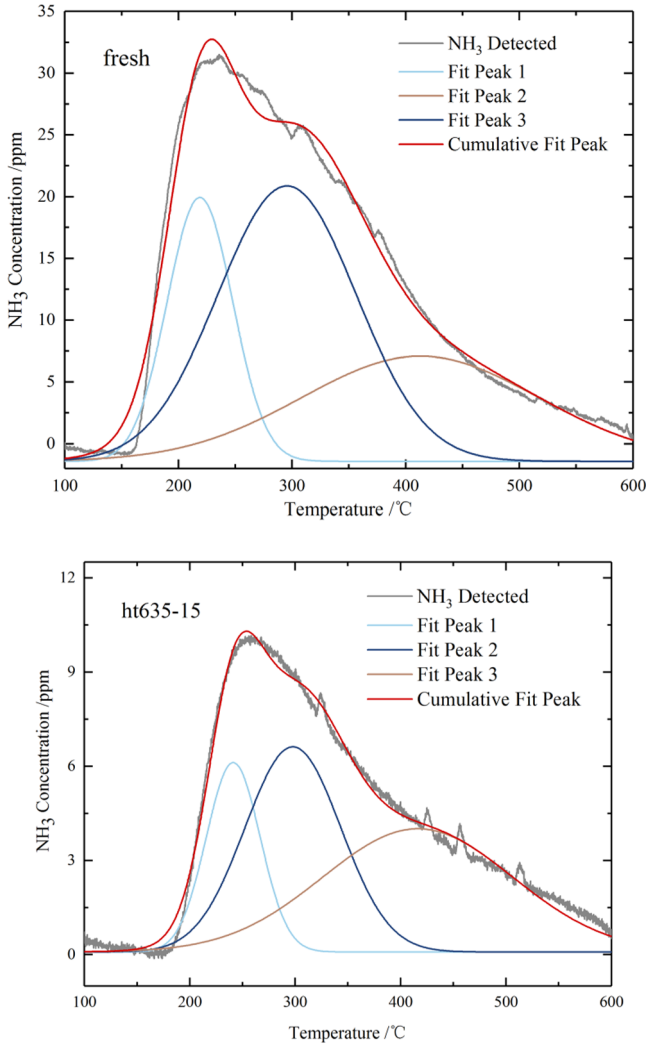

Figure 7. Peak resolution results of ammonia storage tests over a fresh sample and the ht635-15 sample.

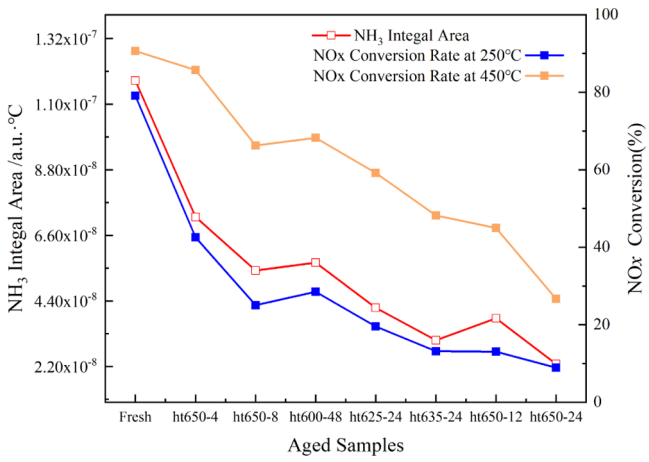

Figure 8. Comparison of the ammonia storage capacity and the NO*x* conversion rate.

To obtain the ammonia storage corresponding to the different active sites of each sample, the NH_3 desorption peaks in the ammonia storage measurement test were integrated, and the ratio of ammonia storage is calculated as follows

$$\text{ratio}_{NH_3} = \frac{NH_3 \text{ integral area}_{aged}}{NH_3 \text{ integral area}_{fresh}} \quad (5)$$

where ratio_{NH_3} represents the ratio of ammonia storage, NH_3 integral area_{aged} represents the ammonia storage of hydrothermally aged samples, and NH_3 integral area_{fresh} represents the ammonia storage of the fresh sample.

Based on the Arrhenius equation, Luo et al.[51] proposed a method considering the ammonia storage rate change of two sites with aging temperature and aging time over Cu-zeolites. We proposed a modified formula to reflect the relationship between the change in ammonia storage of each site and the aging temperature and time over the aged vanadium-based catalyst

$$f(T, t) = \text{ratio}_{NH_3} = -m_1 \cdot \ln\ (T - 200) - m_2 \cdot \ln t + n \quad (6)$$

where $f(T, t)$ represents the regular function of the ammonia storage ratio, T represents the aging temperature, t represents

https://doi.org/10.1021/acsomega.2c06902
ACS Omega 2023, 8, 2421−2434

Table 3. Relationship between Catalyst Particle Size, Specific Surface Area, Ammonia Storage, and NO*x* Conversion Efficiency

NO*x* conversion efficiency	anatase particle diameter	BET specific surface area	ammonia storage
low TEMP stage	0.614	0.981	0.984
high TEMP stage	0.836	0.903	0.971

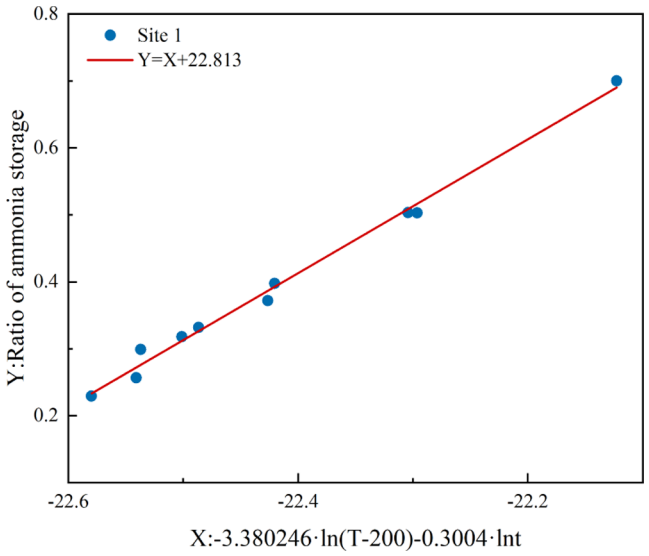

Figure 9. Ammonia storage change of S1 as a function of the aging temperature and time.

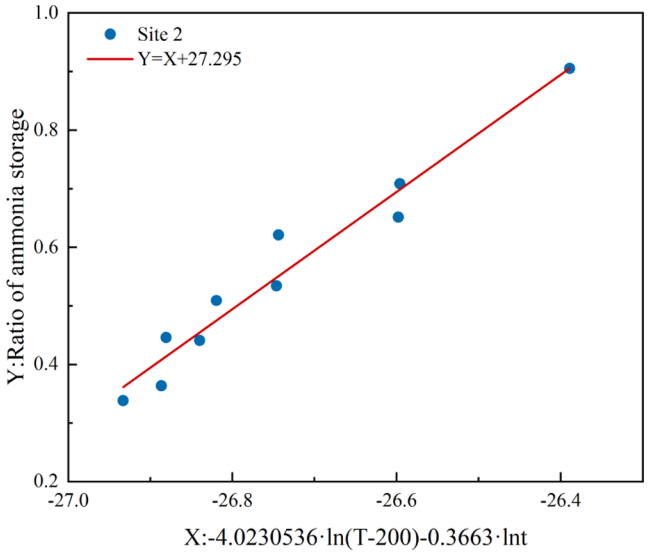

Figure 10. Ammonia storage change of S2 as a function of the aging temperature and time.

the aging time, and m_1, m_2, and n are all dimensionless constants.

After identifying and verifying m_1, m_2, and n, the fitted results are shown in Figures 9 and 10. Equations 7 and 8 represent the ammonia storage change functions of S1 and S2 in the hydrothermal aging process, respectively.

The change function of S1 in the hydrothermal aging process is given as follows

$$f_1(T, t) = -3.38\cdot\ln\ (T - 200) - 0.300\cdot\ln t + 22.8 \tag{7}$$

The change function of S2 in the hydrothermal aging process is given as follows

$$f_2(T, t) = -4.02\cdot\ln(T - 200) - 0.366\cdot\ln t + 27.3 \tag{8}$$

The weighting coefficient of temperature m_1 is greater than the weighting coefficient of aging time m_2, so in the process of hydrothermal aging, the influence of temperature is higher than the influence of aging time, which is consistent with our previous study.[41] The different functions between the two active sites reflect their different sensitivities to hydrothermal aging.

3.2.2. SCR Reactor Modeling. Commercial software MATLAB/Simulink was used to perform the kinetic modeling. A 0D reactor model was developed assuming that the temperature and gas concentrations throughout the control were homogeneous. The mass transfer of the gaseous and surface phase components in the reactions is shown in eqs 9 and 10

$$\varepsilon\cdot\frac{\partial C_{g,i}^n}{\partial t} = -v_g\frac{\partial C_{g,i}^n}{\partial z} - \beta_i A_g(C_{g,i}^n - C_{s,i}^n) \tag{9}$$

$$(1 - \varepsilon)\cdot\frac{\partial C_{s,i}^n}{\partial t} = \beta_i A_g(C_{g,i}^n - C_{s,i}^n) - \sum_j v_{i,j} r_j \tag{10}$$

where ε is the porosity factor of the catalyst, v_g is the flow rate of the exhaust flow, z is the distance of the catalyst sample in the axial space, i represents the gas composition, j represents the reaction of NH_3 adsorption and desorption, NH_3 oxidation, standard SCR, and so on, r_j is the chemical reaction rate, $v_{i,j}$ is the corresponding stoichiometric constant, and A_g is the geometric specific surface area; β_i is the mass transfer coefficient; C_g and C_s represent the gaseous and surface adsorption gas density, respectively.

3.2.3. SCR Reaction Kinetic Modeling. The Arrhenius equation is used to determine the chemical reaction rate

$$r_i = k_i\ \exp\left(-\frac{E_{A,i}}{RT}\right) \tag{11}$$

where i represents the reaction, r_i represents the reaction rate of reaction i, k_i represents the pre-exponential factor of reaction i, and $E_{A,i}$ represents the activation energy of reaction i.

The process of NH_3 adsorption and activation on the catalyst surface is a key part of the entire SCR reaction. NH_3 will be adsorbed in large quantities on the two active sites. The adsorption process is usually regarded as not requiring activation energy. NH_3 desorption adopts the Temkin-type reaction kinetic model.[52] The desorption reaction expression of NH_3 is given in eq 12

$$E_{des,NH_3} = E_{des,NH_3}1 - a_i\Theta_i \tag{12}$$

where Θ_i represents the NH_3 coverage of site i, and a_i represents a constant.

After experimental observation and verification, the rate of NH_3 adsorption and the desorption capacity were found to decrease with the deepening of aging. The aging factor is based on eqs 7 and 8. The initial ratio of Ω_1 and Ω_2 is 1.8. The conversion efficiency of NO*x* in the case of a high NO content mainly depends on the reaction rate of the standard SCR

https://doi.org/10.1021/acsomega.2c06902
ACS Omega 2023, 8, 2421−2434

Table 4. Chemical Reaction Equations and Aging Factors Considered in the Model[a]

no.	reaction	reaction rate
R1	$NH_3 + S_1 \rightarrow S_1 - NH_3$	$r_{ads\_1} = f_1(T,t)\cdot\Omega_1\cdot k_{ads\_1}C_{NH3}\cdot(1-\Theta_1)$
R2	$S_1 - NH_3 \rightarrow NH_3 + S_1$	$r_{des\_1} = f_1(T,t)\cdot\Omega_1\cdot k_{des\_1}\exp\left[-\frac{E_{des\_1}}{RT}(1-a_1\Theta_1)\right]\Theta_1$
R3	$NH_3 + S_2 \rightarrow S_2 - NH_3$	$r_{ads\_2} = f_2(T,t)\cdot\Omega_2\cdot k_{ads\_2}C_{NH3}\cdot(1-\Theta_2)$
R4	$S_2 - NH_3 \rightarrow NH_3 + S_2$	$r_{des\_2} = f_2(T,t)\cdot\Omega_2\cdot k_{des\_2}\exp\left[-\frac{E_{des\_2}}{RT}(1-a_2\Theta_2)\right]\Theta_2$
R5	$S_1 - NH_3 + NO + \frac{1}{4}O_2 \rightarrow N_2 + \frac{3}{2}H_2O + S_1$	$r_{std\_1} = f_1(T,t)\cdot\Omega_1\cdot k_{std\_1}\exp\left(-\frac{E_{std\_1}}{RT}\right)C_{NO}\Theta_1$
R6	$S_2 - NH_3 + NO + \frac{1}{4}O_2 \rightarrow N_2 + \frac{3}{2}H_2O + S_2$	$r_{std\_2} = f_2(T,t)\cdot\Omega_2\cdot k_{std\_2}\exp\left(-\frac{E_{std\_2}}{RT}\right)C_{NO}\Theta_2$
R7	$S_1 - NH_3 + \frac{1}{2}NO + \frac{1}{2}NO_2 \rightarrow N_2 + \frac{3}{2}H_2O + S_1$	$r_{fast\_1} = f_1(T,t)\cdot\Omega_1\cdot k_{fast\_1}\exp\left(-\frac{E_{fast\_1}}{RT}\right)C_{NO}C_{NO2}\Theta_1$
R8	$S_2 - NH_3 + \frac{1}{2}NO + \frac{1}{2}NO_2 \rightarrow N_2 + \frac{3}{2}H_2O + S_2$	$r_{fast\_2} = f_2(T,t)\cdot\Omega_2\cdot k_{fast\_2}\exp\left(-\frac{E_{fast\_2}}{RT}\right)C_{NO}C_{NO2}\Theta_2$
R9	$S_1 - NH_3 + \frac{3}{4}O_2 \rightarrow \frac{1}{2}N_2 + \frac{3}{2}H_2O + S_1$	$r_{NH3\_N2\_1} = 1/f_1(T,t)\cdot\Omega_1\cdot k_{NH3\_N2\_1}\exp\left(-\frac{E_{NH3\_N2\_1}}{RT}\right)\Theta_1\cdot C_{O2}^{0.6}$
R10	$S_1 - NH_3 + \frac{5}{4}O_2 \rightarrow NO + \frac{3}{2}H_2O + S_1$	$r_{NH3\_NO\_1} = 1/f_1(T,t)^K\cdot\Omega_1\cdot k_{NH3\_NO\_1}\exp\left(-\frac{E_{NH3\_N0\_1}}{RT}\right)\Theta_1\cdot C_{O2}^{0.6}$
R11	$S_2 - NH_3 + \frac{3}{4}O_2 \rightarrow \frac{1}{2}N_2 + \frac{3}{2}H_2O + S_2$	$r_{NH3\_N2\_2} = 1/f_2(T,t)\cdot\Omega_2\cdot k_{NH3\_N2\_2}\exp\left(-\frac{E_{NH3\_N2\_2}}{RT}\right)\Theta_2\cdot C_{O2}^{0.6}$
R12	$S_2 - NH_3 + \frac{5}{4}O_2 \rightarrow NO + \frac{3}{2}H_2O + S_2$	$r_{NH3\_NO\_2} = 1/f_2(T,t)^K\cdot\Omega_2\cdot k_{NH3\_NO\_2}\exp\left(-\frac{E_{NH3\_N0\_2}}{RT}\right)\Theta_2\cdot C_{O2}^{0.6}$
R13	$NO + \frac{1}{2}O_2 \rightarrow NO_2$	$r_{NO\_NO2\_1} = f_1(T,t)\cdot k_{NO\_NO2\_1}\exp\left(-\frac{E_{NO\_NO2\_1}}{RT}\right)\cdot C_{O2}^{0.5}C_{NO}$
R14	$NO_2 \rightarrow NO + \frac{1}{2}O_2$	$r_{NO2\_NO\_1} = f_1(T,t)\cdot k_{NO2\_NO\_1}\exp\left(-\frac{E_{NO2\_NO\_1}}{RT}\right)\cdot C_{NO2}$
R15	$NO + \frac{1}{2}O_2 \rightarrow NO_2$	$r_{NO\_NO2\_2} = f_2(T,t)\cdot k_{NO\_NO2\_2}\exp\left(-\frac{E_{NO\_NO2\_2}}{RT}\right)\cdot C_{O2}^{0.5}C_{NO}$
R16	$NO_2 \rightarrow NO + \frac{1}{2}O_2$	$r_{NO2\_NO\_2} = f_2(T,t)\cdot k_{NO2\_NO\_2}\exp\left(-\frac{E_{NO2\_NO\_2}}{RT}\right)\cdot C_{NO2}$

[a]Note: S1, active site 1; S2, active site 2; R1−R4: NH_3 adsorption and desorption; R5−R6: standard SCR; R7−R8: fast SCR; R9−R12: NH_3 oxidation; R13−R16: NO oxidation and NO_2 reduction.

Table 5. Parameter Identification Results of the Activation Energy and Pre-exponential Factor

reaction	activation energy kJ/mol		pre-factor s^{-1}	
r_{ads_1}	E_{ads1}		K_{ads1}	2.75×10^7
r_{des_1}	E_{des1}	65.26	K_{des1}	1.22×10^{10}
r_{ads_1}	E_{ads2}		K_{ads2}	4.31×10^7
r_{des_2}	E_{des2}	54.00	K_{des2}	5.05×10^{10}
r_{std_1}	E_{std1}	89.56	K_{std1}	1.42×10^{11}
r_{std_2}	E_{std2}	95.12	K_{std2}	3.46×10^{12}
r_{fast_1}	E_{fast1}	45.45	K_{fast1}	1.75×10^9
r_{fast_2}	E_{fast2}	53.21	K_{fast2}	8.89×10^9
$r_{NH3\_N2\_1}$	$E_{NH3\_N2\_1}$	165.38	$K_{NH3\_N2\_1}$	7.62×10^{10}
$r_{NH3\_N2\_2}$	$E_{NH3\_N2\_2}$	163.18	$K_{NH3\_N2\_2}$	2.29×10^{12}
$r_{NH3\_NO\_1}$	$E_{NH3\_NO\_1}$	195.53	$K_{NH3\_NO\_1}$	3.90×10^{11}
$r_{NH3\_NO\_2}$	$E_{NH3\_NO\_2}$	216.68	$K_{NH3\_NO\_2}$	2.46×10^{13}
$r_{NO\_NO2\_1}$	$E_{NO\_NO2\_1}$	87.52	$K_{NO\_NO2\_1}$	2.98×10^8
$r_{NO\_NO2\_2}$	$E_{NO\_NO2\_2}$	90.19	$K_{NO\_NO2\_2}$	2.54×10^8
$r_{NO2\_NO\_1}$	$E_{NO2\_NO\_1}$	50.20	$K_{NO2\_NO\_1}$	2.67×10^6
$r_{NO2\_NO\_2}$	$E_{NO2\_NO\_2}$	61.67	$K_{NO2\_NO\_2}$	9.47×10^6

reaction and the fast SCR reaction. The change in ammonia storage shows the highest correlation with the conversion efficiency of NOx. Therefore, after verification, the aging factors corresponding to the standard SCR reaction and the fast SCR reaction can be determined by eqs 7 and 8. For vanadium-based catalysts, with an increase in the aging temperature, the proportion of NH_3 oxidation side reactions shows an increasing trend. After fitting and verification, it is concluded that the aging factor of NH_3 oxidation to N_2 on S1 is $1/f_1(T,t)$, the aging factor of NH_3 oxidation to N_2 on S2 is $1/f_2(T,t)$, the aging factor of NH_3 oxidation to NO on S1 is $1/f1(T,t)^K$, and the aging factor of NH_3 oxidation to NO on S2 is $1/f_2(T,t)^K$. K is the aging factor correction parameter, which requires parameter identification. For the reversible reaction between NO and NO_2, the aging factor can also be expressed by eqs 7 and 8. The complete chemical reaction rate equation and corresponding aging factor are shown in Table 4.

3.3. Model Parameter Identification and Verification.

3.3.1. Reaction Kinetic Parameter Identification. After the reaction kinetics test, six samples were selected for parameter identification: the fresh sample and hydrothermally aged samples ht635-6, ht635-9, ht635-11, ht635-15, and ht625-15. The parameter identification toolbox was used for parameter identification. The parameter identification algorithm used the least-squares method. In the Simulink parameter identification, the variable step size setting was adopted, the simulation time was 61,660 s, the maximum number of iterations was 500, and the convergence accuracy was 0.001. The input included the aging time, aging temperature, test temperature in the reaction kinetics test of different aging samples, and concentrations of NH_3, NO, NO_2, H_2O, and O_2.

As shown in Table 5, after the above parameter identification process, all of the activation energy and pre-exponential factor results of the reaction kinetics equation and the material balance equation were obtained. Besides, Ω_1 and Ω_2 are the initial active site densities, and their values are 103.11 and 54.84 mol/m^3, respectively. ε is a constant, and its value is 0.4. The values of a_1 and a_2 are 0.752 and 0.665, respectively. The identification result of the correction parameter K for the aging factor of NH_3 oxidation to NO is 2.01.

https://doi.org/10.1021/acsomega.2c06902
ACS Omega 2023, 8, 2421−2434

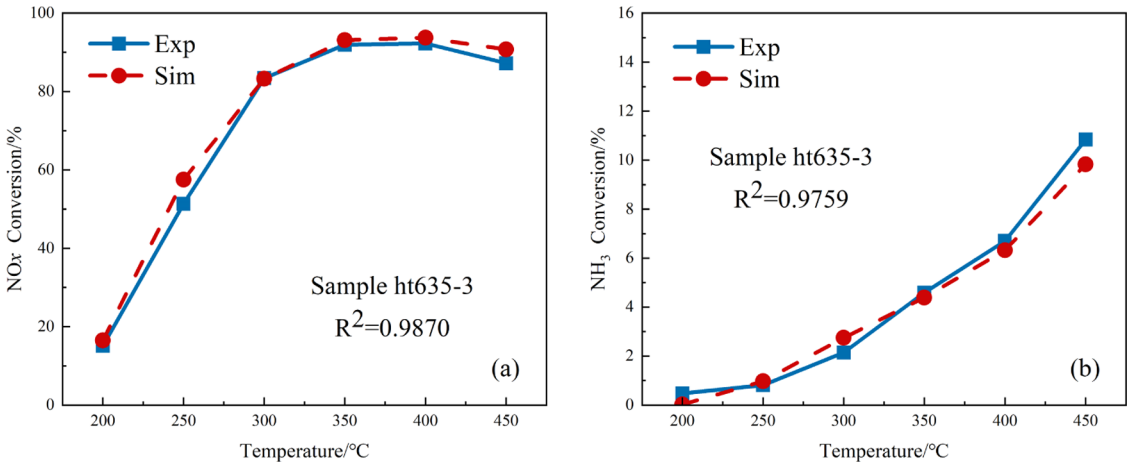

Figure 11. Comparison between simulation and experimental results of sample ht635-3: (a) NO*x* conversion rate; (b) NH_3 conversion rate.

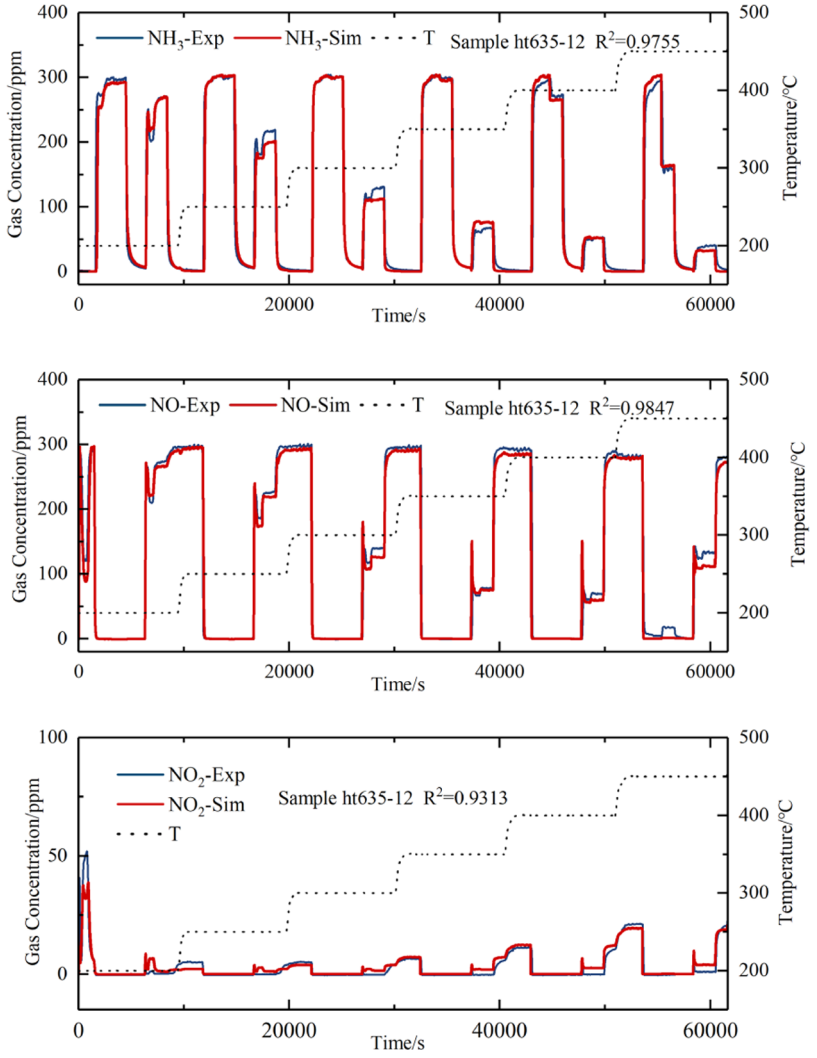

Figure 12. Comparison between transient simulation results and experimental results of NH_3, NO, and NO_2 over sample ht635-12.

3.3.2. Model Steady-State and Transient Verification. After determining the parameters of the hydrothermal aging reaction kinetic model, the model was further verified. Six samples were selected for parameter identification: ht635-3, ht635-12, ht600-15, ht615-15, ht630-15, and ht-diff-tT.

For the samples aged at the same temperature, ht635-3 and ht635-12 were used to represent mild and moderate hydrothermal aging, respectively, and the steady-state and transient verifications were carried out. Steady-state verification was carried out by measuring NO*x* conversion and NH_3 conversion between 200 and 450 °C on ht635-3 sample. The NO*x* and

https://doi.org/10.1021/acsomega.2c06902
ACS Omega 2023, 8, 2421−2434

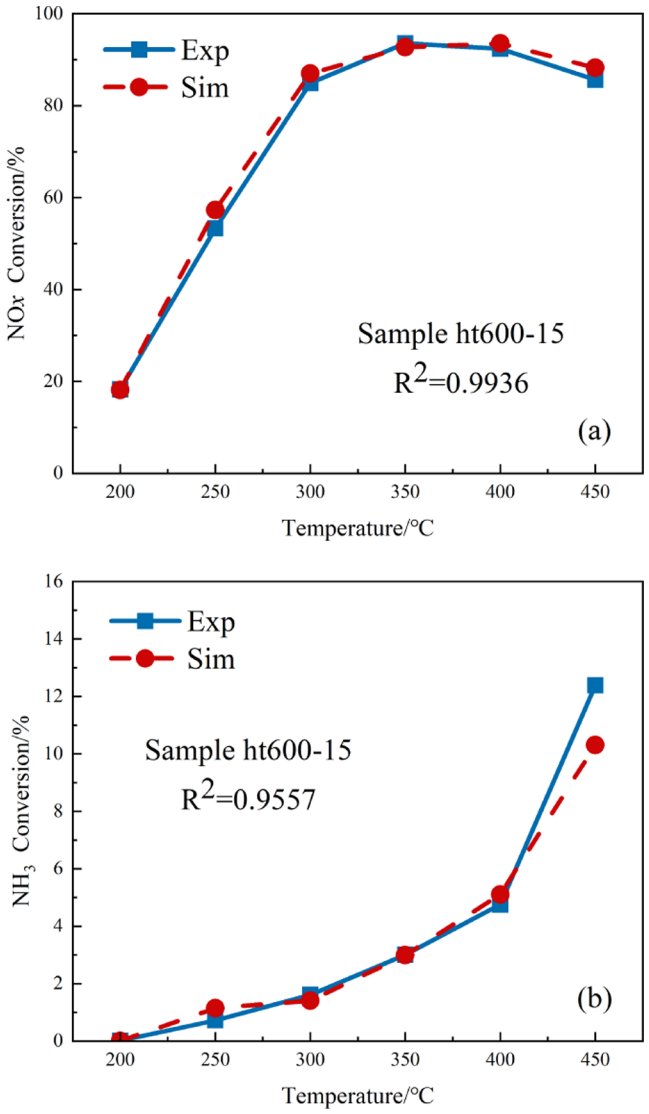

Figure 13. Comparison between simulation results and experimental results of sample ht600-15: (a) NO*x* conversion rate; (b) NH_3 conversion rate.

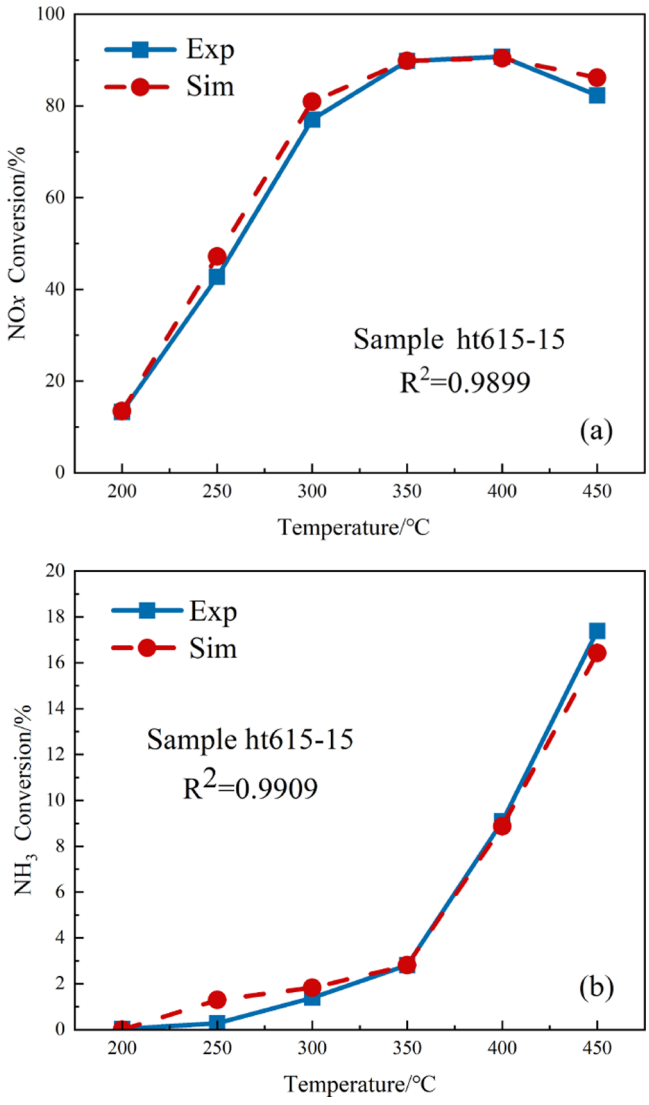

Figure 14. Comparison between simulation results and experimental results of sample ht615-15: (a) NO*x* conversion rate; (b) NH_3 conversion rate.

NH_3 conversion rates were calculated according to eqs 3 and 4, respectively. In Figure 11, the coefficients of determination of the NO*x* and NH_3 conversion rates of the sample ht635-3 are both greater than 0.97, indicating that the simulation error of the standard SCR reaction in the steady-state stage of the aged sample is low.

Transient verification of the performance evaluation process of the sample ht635-12 is shown in Figure 12, and the determination coefficients of all gas components are greater than 0.93. The error of simulation mainly occurs at 450 °C. Although it can be seen that the concentration of NH_3 at 450 °C is in good agreement, the NO formed by the oxidation of NH_3 could not be accurately simulated. The aging factor itself has certain errors in the high-temperature section, which may lead to inaccurate simulation results in the same section. As a result of the high aging degree of the sample, the proportion of side reactions in the high-temperature section increases.

The steady-state verification results of the samples under the same aging time are shown in Figures 13 and 14, and the samples are ht600-15 and ht615-15, respectively; the transient verification results are shown in Figure 15, and the sample is ht630-15. For samples ht600-15 and ht615-15 verified in the steady state, the determination coefficient of the NO*x* conversion efficiency is as high as 0.99, and the reason for the error in the NH_3 oxidation process is consistent with the previous analysis.

As shown in Figure 15, for the sample ht630-15 used for transient verification, the highest conversion efficiency is about 72.63%. The determination coefficient for NH_3 concentration was 0.9686, and the determination coefficient for NO concentration was 0.9806, which indicates good fitting accuracy.

In addition to the above verifications, we also verified the multistage hydrothermal aging. The samples used for validation were first aged at 600 °C for 6 h, then at 625 °C for 5 h, and finally at 650 °C for 4 h (ht-diff-tT). The simulation results and experimental results of the ht-diff-tT sample are shown in Figure 16. The comparison between the simulated value and the measured value shows that the accuracy of the simulation is very good, and the determination coefficients of NO and NH_3 are both higher than 0.96.

https://doi.org/10.1021/acsomega.2c06902
ACS Omega 2023, 8, 2421−2434

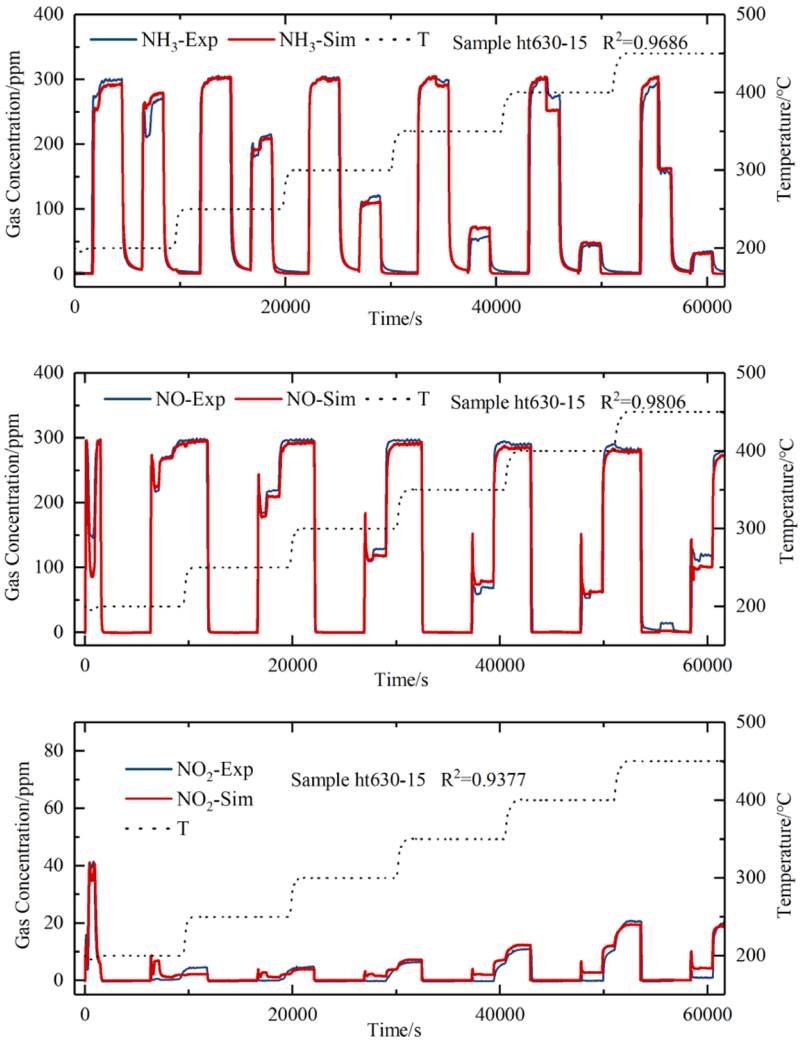

Figure 15. Comparison between transient simulation results and experimental results of NH_3, NO, and NO_2 over sample ht630-15.

In summary, the hydrothermal aging kinetic model established in this study is suitable for aging samples with different aging temperatures and different aging times. It is reasonable and accurate to use the change rule of the ratio of ammonia storage as the aging factor in the aging process. The kinetic modeling of the hydrothermal aging reaction for vanadium-based catalysts considers two active sites that are affected by the aging temperature and aging time differently. The model constructed in this study is suitable for predicting catalysts with a moderate aging degree, and the prediction accuracy for NO and NH_3 concentrations is greater than 0.95. When the catalyst has extremely deteriorated, the proportion of side reactions and products at high temperature changes, and the macroscopic performance of the powdered catalyst also changes, which affects the measurement accuracy of the experiment, and the error at high temperature will increase.

4. CONCLUSIONS

In this study, the hydrothermal aging mechanism of vanadium-based catalysts was explored, and the microscopic mechanism was applied to establish a hydrothermal aging reaction kinetics model of dual active sites.

The NO*x* conversion rate of the catalyst samples after hydrothermal aging decreased sharply, and the temperature window was greatly reduced; when the aging temperature reached a certain value, the NO*x* conversion rate was very sensitive to an increase in the hydrothermal aging temperature. The higher the aging temperature, the greater its effect on conversion. Moreover, the sensitivity of the NO*x* conversion rate at different temperatures is different. The relative deactivation degree at lower temperatures is relatively high at the beginning, and the subsequent growth slows down, while the relative deactivation rate at higher temperatures is low in the beginning and then gradually increases. Therefore, considering the relative inactivation degree of different temperature sections, it can also be divided into the high-temperature section (around 400 °C) and the low-temperature section (around 250 °C).

In the process of hydrothermal aging, the sintering of the catalyst carrier and the growth of particles will occur, so that the dispersion of vanadium species deteriorates, the specific surface area of the catalyst decreases, and the number and distribution of active sites are indirectly affected. Comparing the correlations between the carrier particle size, specific surface area, ammonia storage capacity, and NO*x* conversion efficiency, the ammonia storage amount shows the highest correlation with the NO*x* conversion efficiency. In the process of hydrothermal aging, the essence of deactivation is the reduction of catalyst active sites. The change law of the number of active sites can be characterized by the change law

https://doi.org/10.1021/acsomega.2c06902
ACS Omega 2023, 8, 2421−2434

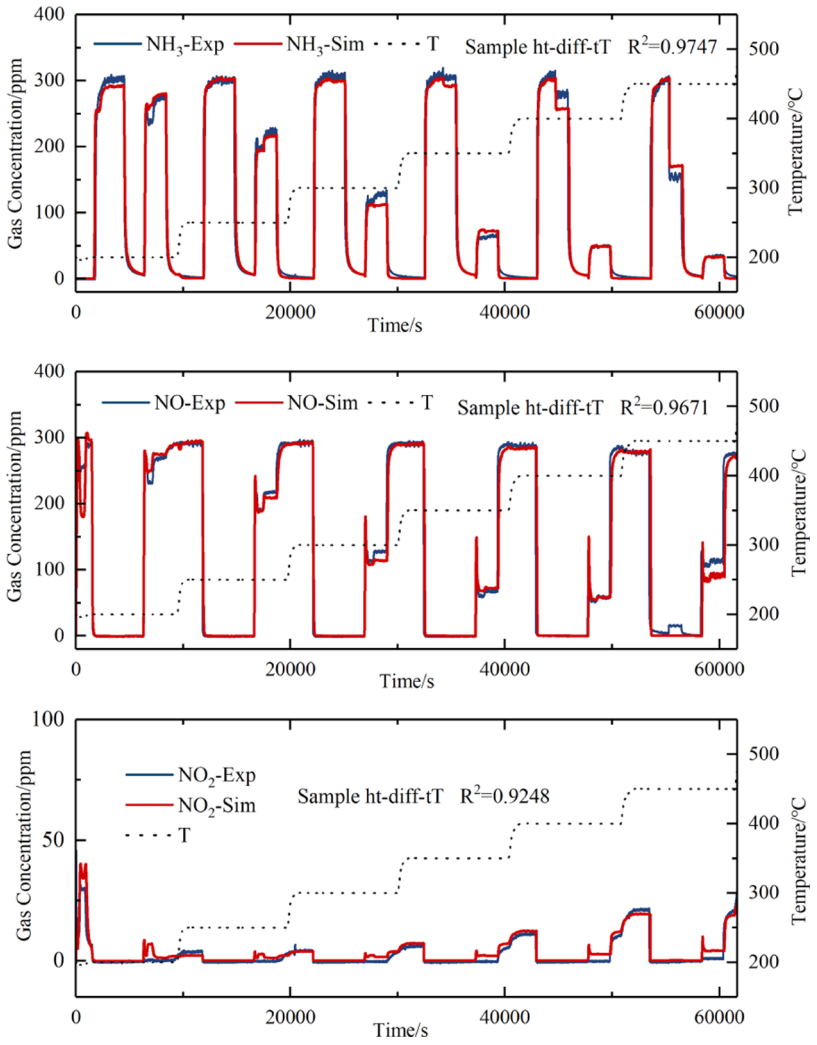

Figure 16. Comparison between transient simulation results and experimental results of NH_3, NO, and NO_2 over the sample ht-diff-tT.

of ammonia storage capacity during the aging process. As a result of the different sensitivities of the Lewis and the Brønsted acid sites to hydrothermal aging over vanadium-based catalysts, their capacities decrease differently and the ratio of active sites changes. This explains the difference in the relative deactivation degree of the catalyst in the high-temperature and low-temperature sections after hydrothermal aging.

The ammonia storage test was carried out on the samples after hydrothermal aging, and the obtained NH_3 desorption peaks were separated. The integral areas of different temperature sections represent different active sites, and the change functions of different active sites during hydrothermal aging were obtained. Using this law as the aging factor, a hydrothermal aging kinetic model of dual active sites was established. For NH_3 adsorption and desorption, standard SCR reaction, fast SCR reaction, and NO oxidation reaction, the chemical reaction rate equations are multiplied by the aging factors to characterize the aging reaction rate equations. The accuracy and universality of the model are verified from multiple perspectives, including isothermal aging, isochronous aging, and multistage aging samples.

AUTHOR INFORMATION

Corresponding Author

Dongwei Yao − *College of Energy Engineering, Zhejiang University, Hangzhou 310027, China; Key Laboratory of Smart Thermal Management Science & Technology for Vehicles of Zhejiang Province, Taizhou 317200, China;* orcid.org/0000-0001-7698-514X; Email: dwyao@zju.edu.cn

Authors

Xiaohan Hu − *College of Energy Engineering, Zhejiang University, Hangzhou 310027, China*

Feng Wu − *College of Energy Engineering, Zhejiang University, Hangzhou 310027, China*

Xingwen Li − *College of Energy Engineering, Zhejiang University, Hangzhou 310027, China;* orcid.org/0000-0003-2429-8617

Yuxi Li − *College of Energy Engineering, Zhejiang University, Hangzhou 310027, China*

Complete contact information is available at: https://pubs.acs.org/10.1021/acsomega.2c06902

Notes

The authors declare no competing financial interest.

https://doi.org/10.1021/acsomega.2c06902
ACS Omega 2023, 8, 2421−2434

■ ACKNOWLEDGMENTS

This study was financially supported by the National Natural Science Foundation of China [grant number 52176135 & 52276136] and the National Key R&D Plan of China [grant number 2016YFC0207905, 2017YFC0211101 & 2017YFC0211103]. The authors also thank the China National Heavy Duty Truck Group Co. Ltd. for providing the commercial V_2O_5-WO_3/TiO_2 catalyst samples.

■ REFERENCES

(1) Mwangi, J. K.; Lee, W. J.; Chang, Y. C.; Chen, C. Y.; Wang, L. C. An overview: Energy saving and pollution reduction by using green fuel blends in diesel engines. *Appl. Energy* **2015**, *159*, 214−236.
(2) Jiang, K.; Cao, E.; Wei, L. NOx sensor ammonia cross-sensitivity estimation with adaptive unscented Kalman filter for Diesel-engine selective catalytic reduction systems. *Fuel* **2016**, *165*, 185−192.
(3) Maunula, T.; Viitanen, A.; Kinnunen, T.; Kanniainen, K. In *Design of Durable Vanadium - SCR Catalyst Systems for Heavy - Duty Diesel Applications*; Symposium on International Automotive Technology; The Automotive Research Association of India, 2013; p 11.
(4) Aguilar-Romero, M.; Camposeco, R.; Castillo, S.; Marin, J.; Rodriguez-González, V.; Garcia-Serrano, L. A.; Mejia-Centeno, I. Acidity, surface species, and catalytic activity study on V_2O_5-WO_3/TiO_2 nanotube catalysts for selective NO reduction by NH_3. *Fuel* **2017**, *198*, 123−133.
(5) Li, F.; Shen, B.; Tian, L.; Li, G.; He, C. Enhancement of SCR activity and mechanical stability on cordierite supported V_2O_5-WO_3/TiO_2 catalyst by substrate acid pretreatment and addition of silica. *Powder Technol.* **2016**, *297*, 384−391.
(6) Alemany, L. J.; Berti, F.; Busca, G.; Ramis, G.; Robba, D.; Toledo, G. P.; Trombetta, M. Characterization and composition of commercial V_2O_5-WO_3-TiO_2 SCR catalyst. *Appl. Catal., B* **1996**, *10*, 299−311.
(7) Guan, B.; Zhan, R.; Lin, H.; Huang, Z. Review of state of the art technologies of selective catalytic reduction of NOx from diesel engine exhaust. *Appl. Therm. Eng.* **2014**, *66*, 395−414.
(8) Zardini, A.; Giechaskiel, B.; Martini, G.*Durability Demonstration Programme for Euro 6 Passenger Cars: Thermal Load to After-Treatment Systems*. Final report. EUR 29278 EN; Publications Office of the European Union: Luxembourg; 2018. ISBN 978-92-79-88014-8.
(9) Maunula, T.; Kinnunen, T.; Kanniainen, K.; Viitanen, A.; Savimaki, A. In *Thermally Durable Vanadium-SCR Catalysts for Diesel Applications*; SAE 2013 World Congress & Exhibition; SAE International, 2013; Vol. 2, p 10.
(10) Xi, Y.; A Ottinger, N.; Liu, Z. G.*Effect of Hydrothermal Aging on the Catalytic Performance and Morphology of a Vanadia SCR Catalyst*; SAE 2013 World Congress & Exhibition; SAE International, 2013; p 10.
(11) Madia, G.; Elsener, M.; Koebel, M.; Raimondi, F.; Wokaun, A. Thermal stability of vanadia-tungsta-titania catalysts in the SCR process. *Appl. Catal., B* **2002**, *39*, 181−190.
(12) Beale, A. M.; Lezcano-Gonzalez, I.; Maunula, T.; Palgrave, R. G. Development and characterization of thermally stable supported V−W−TiO_2 catalysts for mobile NH_3−SCR applications. *Catal., Struct. React.* **2014**, *1*, 25−34.
(13) Went, G. T.; Leu, L.-J.; Rosin, R. R.; Bell, A. T. The effects of structure on the catalytic activity and selectivity of V_2O_5/TiO_2 for the reduction of NO by NH_3. *J. Catal.* **1992**, *134*, 492−505.
(14) Reddy, B. M.; Ganesh, I.; Reddy, E. P. Study of Dispersion and Thermal Stability of V_2O_5/TiO_2-SiO_2 Catalysts by XPS and Other Techniques. *J. Phys. Chem. B* **1997**, *101*, 1769−1774.
(15) Choung, J. W.; Nam, I.-S.; Ham, S.-W. Effect of promoters including tungsten and barium on the thermal stability of V_2O_5/sulfated TiO_2 catalyst for NO reduction by NH_3. *Catal. Today* **2006**, *111*, 242−247.
(16) Went, G. T.; Leu, L.-j.; Bell, A. T. Quantitative structural analysis of dispersed vanadia species in TiO_2(anatase)-supported V_2O_5. *J. Catal.* **1992**, *134*, 479−491.
(17) Wachs, I. E.; Deo, G.; Weckhuysen, B. M.; Andreini, A.; Vuurman, M. A.; de Boer, M.; Amiridis, M. D. Selective Catalytic Reduction of NO with NH_3 over Supported Vanadia Catalysts. *J. Catal.* **1996**, *161*, 211−221.
(18) Djerad, S.; Tifouti, L.; Crocoll, M.; Weisweiler, W. Effect of vanadia and tungsten loadings on the physical and chemical characteristics of V_2O_5-WO_3/TiO_2 catalysts. *J. Mol. Catal. A: Chem.* **2004**, *208*, 257−265.
(19) Lai, J.-K.; Wachs, I. E. A Perspective on the Selective Catalytic Reduction (SCR) of NO with NH3 by Supported V_2O_5−WO_3/TiO_2 Catalysts. *ACS Catal.* **2018**, *8*, 6537−6551.
(20) Chen, L.; Li, J.; Ge, M.-F. DRIFT Study on Cerium- Tungsten/Titiania Catalyst for Selective Catalytic Reduction of NOx with NH_3. *Environ. Sci. Technol.* **2010**, *44*, 9590−9596.
(21) Nova, I.; dall'Acqua, L.; Lietti, L.; Giamello, E.; Forzatti, P. Study of thermal deactivation of a de-NOx commercial catalyst. *Appl. Catal., B* **2001**, *35*, 31−42.
(22) Ramis, G.; Yi, L.; Busca, G. Ammonia activation over catalysts for the selective catalytic reduction of NOx and the selective catalytic oxidation of NH3. An FT-IR study. *Catal. Today* **1996**, *28*, 373−380.
(23) Topsøe, N. Y. Mechanism of the Selective Catalytic Reduction of Nitric Oxide by Ammonia Elucidated by in Situ On-Line Fourier Transform Infrared Spectroscopy. *Science* **1994**, *265*, 1217−1219.
(24) Topsøe, N.-Y.; Topsøe, H.; Dumesic, J. A. Vanadia/Titania Catalysts for Selective Catalytic Reduction (SCR) of Nitric-Oxide by Ammonia: I. Combined Temperature-Programmed in-Situ FTIR and On-line Mass-Spectroscopy Studies. *J. Catal.* **1995**, *151*, 226−240.
(25) Zhu, M.; Lai, J.-K.; Tumuluri, U.; Wu, Z.; Wachs, I. E. Nature of Active Sites and Surface Intermediates during SCR of NO with NH3 by Supported V_2O_5-WO_3/TiO_2 Catalysts. *J. Am. Chem. Soc.* **2017**, *139*, 15624−15627.
(26) Liu, H.; You, C.; Wang, H. Time-resolved in-situ IR and DFT study: NH_3 adsorption and redox cycle of acid site on vanadium-based catalysts for NO abatement via selective catalytic reduction. *Chem. Eng. J.* **2020**, *382*, No. 122756.
(27) Song, I.; Lee, H.; Jeon, S. W.; Kim, D. H. Understanding the dynamic behavior of acid sites on TiO_2-supported vanadia catalysts via operando DRIFTS under SCR-relevant conditions. *J. Catal.* **2020**, *382*, 269−279.
(28) Nova, I.; Tronconi, E. Kinetic Study of the NO/NO_2-NH_3 SCR Reactions Over a $V_2O_5WO_3$/TiO_2 Commercial Catalyst for the after Treatment of Diesel Engines Exhausts. *IFAC Proc. Vol.* **2009**, *42*, 183−190.
(29) Nova, I.; Ciardelli, C.; Tronconi, E.; Chatterjee, D.; Weibel, M. NH_3-NO/NO_2 SCR for diesel exhausts after treatment: mechanism and modelling of a catalytic converter. *Top. Catal.* **2007**, *42*−*43*, 43−46.
(30) Nova, I.; Ciardelli, C.; Tronconi, E.; Chatterjee, D.; Bandl-Konrad, B. NH_3-SCR of NO over a V-based catalyst: Low-T redox Kinetics with NH_3 inhibition. *AIChE J.* **2006**, *52*, 3222−3233.
(31) Nova, I.; Tronconi, E.*Urea-SCR Technology for deNOx After Treatment of Diesel Exhausts*, 1st ed.; Springer: New York, 2014; p XX, 716.
(32) Tronconi, E.; Nova, I.; Ciardelli, C.; Chatterjee, D.; Weibel, M. Redox features in the catalytic mechanism of the ″standard″ and ″fast″ NH_3-SCR of NOx over a V-based catalyst investigated by dynamic methods. *J. Catal.* **2007**, *245*, 1−10.
(33) Yun, B. K.; Kim, M. Y. Modeling the selective catalytic reduction of NOx by ammonia over a Vanadia-based catalyst from heavy duty diesel exhaust gases. *Appl. Therm. Eng.* **2013**, *50*, 152−158.
(34) Lothongkum, A. W.; Sethapokin, P.; Ouraipryvan, P. Simulation of V_2O_5/TiO_2 catalyst activity by central composite design for optimal operating conditions and catalyst life in phthalic anhydride production. *J. Ind. Eng. Chem.* **2015**, *25*, 288−294.
(35) Yu, C.; Zhang, B.; Fan, W.; Ren, S.; Li, S.; Jiang, X.; Si, F. 1D kinetic analysis and 3D multi-channel modeling of plate-type monolithic catalysts for a Selective Catalytic Reduction process. *Energy Procedia* **2017**, *136*, 182−187.

https://doi.org/10.1021/acsomega.2c06902
ACS Omega 2023, 8, 2421−2434

(36) Usberti, N.; Jablonska, M.; Blasi, M. D.; Forzatti, P.; Lietti, L.; Beretta, A. Design of a "high-efficiency" NH_3-SCR reactor for stationary applications. A kinetic study of NH_3 oxidation and NH_3-SCR over V-based catalysts. *Appl. Catal., B* **2015**, *179*, 185−195.
(37) Beretta, A.; Lanza, A.; Lietti, L.; Alcove, S.; Collier, J.; Nash, M. An investigation on the redox kinetics of NH_3-SCR over a V/Mo/Ti catalyst: Evidence of a direct role of NO in the re-oxidation step. *Chem. Eng. J.* **2019**, *359*, 88−98.
(38) Shin, S. B.; Skau, K. I.; Menon, M.; Maroor, S.; Spatenka, S. A modelling approach to kinetics study and novel monolith channel design for selective catalytic reduction (SCR) applications. *Chem. Eng. Res. Des.* **2019**, *142*, 412−428.
(39) Xiong, S.; Xiao, X.; Liao, Y.; Dang, H.; Shan, W.; Yang, S. Global Kinetic Study of NO Reduction by NH_3 over V_2O_5−WO_3/TiO_2: Relationship between the SCR Performance and the Key Factors. *Ind. Eng. Chem. Res.* **2015**, *54*, 11011−11023.
(40) Soleimanzadeh, H.; Niaei, A.; Salari, D.; Tarjomannejad, A.; Penner, S.; Grünbacher, M.; Hosseini, S. A.; Mousavi, S. M. Modeling and optimization of V_2O_5 /TiO_2 nanocatalysts for NH_3 -Selective catalytic reduction (SCR) of NOx by RSM and ANN techniques. *J. Environ. Manage.* **2019**, *238*, 360−367.
(41) Li, X.; Yao, D.; Wu, F.; Wang, X.; Wei, L.; Liu, B. New Findings in Hydrothermal Deactivation Research on the Vanadia-Selective Catalytic Reduction Catalyst. *ACS Omega* **2019**, *4*, 5088−5097.
(42) Bartley, G. J.; Chadwell, C. J.; Kostek, T. M.; Zhan, R.*SCR Deactivation Kinetics for Model-Based Control and Accelerated Aging Applications*, SAE 2012 World Congress & Exhibition; SAE International, 2012; p 6.
(43) Kim, J. Y.; Cavataio, G.; Patterson, J. E.; Laing, P. M.; Lambert, C. K.*Laboratory Studies and Mathematical Modeling of Urea SCR Catalyst Performance*, SAE World Congress & Exhibition; SAE International, 2007; p 12.
(44) Kim, J. Y.; Cheng, Y.; Patterson, J. E.; Laing, P. M.; Lambert, C. K.*Modeling Study of Urea SCR Catalyst Aging Characteristics*, SAE World Congress & Exhibition; SAE International, 2007; p 11.
(45) Supriyanto; Wijayanti, K.; Kumar, A.; Joshi, S.; Kamasamudram, K.; Currier, N. W.; Yezerets, A.; Olsson, L. Global kinetic modeling of hydrothermal aging of NH_3-SCR over Cu-zeolites. *Appl. Catal., B* **2015**, *163*, 382−392.
(46) Yang, R.; Huang, H.; Chen, Y.; Zhang, X.; Lu, H. Performance of Cr-doped vanadia/titania catalysts for low-temperature selective catalytic reduction of NOx with NH_3. *Chin. J. Catal.* **2015**, *36*, 1256−1262.
(47) Hu, S.; Gong, Y.; Xu, Q.; Liu, X.; Zhang, Q.; Zhang, L.; Dou, T. Highly selective formation of propylene from methanol over high-silica EU-1 zeolite catalyst. *Catal. Commun.* **2012**, *28*, 95−99.
(48) Du, Z.; Fu, Y.; Zhu, Y. Study of poisoning mechanism for V_2O_5 /TiO_2 catalyst. *Huanjing Kexue Xuebao/ Acta Sci. Circumstantiae* **2013**, *33*, 216−223.
(49) Tang, F.; Zhuang, K.; Yang, F.; Yang, L.; Xu, B.; Qiu, J.; Fan, Y. Effect of Dispersion State and Surface Properties of Supported Vanadia on the Activity of V_2O_5/TiO_2 Catalysts for the Selective Catalytic Reduction of NO by NH_3. *Chin. J. Catal.* **2012**, *33*, 933−940.
(50) Lin, C. H.; Bai, H. Surface acidity over vanadia/titania catalyst in the selective catalytic reduction for NO removal-in situ DRIFTS study. *Appl. Catal., B* **2003**, *42*, 279−287.
(51) Luo, J.; Kamasamudram, K.; Currier, N.; Yezerets, A. NH_3 -TPD methodology for quantifying hydrothermal aging of Cu/SSZ-13 SCR catalysts. *Chem. Eng. Sci.* **2018**, *190*, 60−67.
(52) Lietti, L.; Nova, I.; Camurri, S.; Tronconi, E.; Forzatti, P. Dynamics of the SCR-DeNOx reaction by the transient-response method. *AIChE J.* **1997**, *43*, 2559−2570.

https://doi.org/10.1021/acsomega.2c06902
ACS Omega 2023, 8, 2421−2434